Available online at www.sciencedirect.com

ScienceDirect

Ceramics International 40 (2014) 297–305

CERAMICS INTERNATIONAL

www.elsevier.com/locate/ceramint

Crystallization and sinterability of glass-ceramics in the system La_2O_3–SrO–B_2O_3

Sonja V. Smiljanić[a,*], Snežana R. Grujić[a], Mihajlo B. Tošić[b], Vladimir D. Živanović[b], Jovica N. Stojanović[b], Srdjan D. Matijašević[b], Jelena D. Nikolić[b]

[a]*Faculty of Technology and Metallurgy, Karnegijeva 4, University of Belgrade, 11000 Belgrade, Serbia*
[b]*Institute for the Technology of Nuclear and Other Raw Materials, 86 Franchet d'Esperey St, 11000 Belgrade, Serbia*

Received 20 March 2013; received in revised form 24 May 2013; accepted 1 June 2013
Available online 15 June 2013

Abstract

Glasses with a constant B_2O_3 and an increasing La_2O_3 content in the system La_2O_3–SrO–B_2O_3 were obtained by the usual melt quenching procedure. The crystallization and sinterability of the glasses were investigated by hot stage microscopy (HSM), differential thermal analysis (DTA), X-ray diffraction (XRD) analysis, transmission electron microscopy (TEM) and scanning electron microscopy (SEM). XRD analysis of the bulk samples evidenced the formation of the crystalline phases: $La_2SrB_{10}O_{19}$, SrB_6O_{10} and $SrLaBO_4$. XRD and TEM/SAED analyses showed a polymorphic crystallization of the glass sample containing 14.3 mol% La_2O_3 with precipitation of the $La_2SrB_{10}O_{19}$ phase. SEM analysis confirmed the surface crystallization mechanism of this sample. The kinetics of crystallization of the same sample was examined by DTA and the activation energy of crystal growth was calculated by the Kissinger model to be $E_a = 458 \pm 63$ kJ mol^{-1}.

Keywords: A. Sintering; B. Electron microscopy; D. Glass; Glass-ceramics

1. Introduction

Glass-ceramics materials show good properties, such as: low thermal expansion, low dielectric constant, high abrasion resistance and chemical resistance [1]. The specific properties of these ceramics materials recommend glass-ceramics for numerous applications [1,2]. Glass-ceramics can be formed from the bulk glass through the processes of controlled nucleation and crystallization by adequate heat treatment. Regarding the preparation of glass-ceramics with desired microstructure and properties using this method, the determination of the parameters for these two processes is crucial. The crystalline phase formed by the process of crystallization in the glass determines specific properties of glass-ceramics. Lanthanide borate glasses and glass-ceramics are recognized as materials for the application as laser hosts, nonlinear optical materials, and in the optoelecrtonics. Lanthanide materials showed improved NLO properties which are explained by the f–f electron transition. [3–6]. Addition of lanthanum oxide in the alkaline earth borate glasses improves optical properties and chemical durability [7].

The glass-ceramics can be also obtained through the sintering and crystallization of glass powder [8–10]. It is preferable that densification is performed prior to the crystallization; hence these processes are independent. The quality of the obtained glass-ceramics material is determined by the densification of the glass powder compact [11–13]. Lanthanide alkaline borate glasses showed improved durability and high glass-transition temperatures, due to that these glasses can be applied as specialized hermetic candidates [14]. These glasses are also potential candidates for the application in various electronic industries such as display panels, low-temperature co-fired ceramics and packaging where there is requirement for the low-temperature sinterable glasses [15,16].

The crystallization behavior of glasses from the ternary system La_2O_3–CaO–B_2O_3 was previously the subject of investigation and the crystalline phase $La_2CaB_{10}O_{19}$ with the desired properties was identified after heat treatment of these glasses [4–6].

The sintering and crystallization behavior of the glasses from the La_2O_3–SrO–B_2O_3 system, to the best of our

*Corresponding author.
E-mail addresses: szdrale@tmf.bg.ac.rs, sonja.smiljanic@yahoo.com (S.V. Smiljanić).

0272-8842/$ - see front matter © 2013 Elsevier Ltd and Techna Group S.r.l. All rights reserved.
http://dx.doi.org/10.1016/j.ceramint.2013.06.002

Table 1
Compositions of the glass samples.

Glass sample	La_2O_3	x_i (mol%) SrO	B_2O_3
GLa5.7	5.7	22.9	71.4
GLa9.5	9.5	19.1	71.4
GLa14.3	14.3	14.3	71.4
GLa19.1	19.1	9.5	71.4

knowledge, have not been studied in detail. The aim of this study was to investigate the processes of sintering and crystallization of the glass system La_2O_3–SrO–B_2O_3 under isothermal and non-isothermal conditions.

2. Experimental

Glasses with different compositions (Table 1) were obtained by the usual melt quenching procedure. Reagent-grade H_3BO_3, $SrCO_3$ and $La_2(CO_3)_3$ were mixed and homogenized. The mixture was placed in a platinum crucible in an electric furnace and melted at 1200 °C for 30 min. The platinum crucible was covered, melting was in short time at relatively low melting temperatures to minimize boron evaporation. The melt was cast and cooled on a stainless steel plate in air at room temperature. Measurements of the weight loss due to melting indicate that the glasses are within 1–2 wt% of desired compositions. The obtained glass samples were transparent, without visible bubbles. X-Ray powder diffraction (XRD) measurements confirmed that the samples were amorphous. Differential thermal analysis (DTA) and hot stage microscopy (HSM), and a combination of these two techniques, were used for the investigation of crystallization and sintering behavior of the glass powder samples. Glass powder samples were prepared by crushing and grinding the bulk glass in an agate mortar and sieving it to grain size < 0.048 mm. DTA curves were recorded on a Netzsch STA 409 EP instrument at different heating rates 5, 10, 12 and 20 °C min^{-1}, using Al_2O_3 powder as the reference material and 100 mg of glass powder. From the DTA curves, the glass transition, T_g, crystallization onset, T_x, and crystallization peak, T_p, temperatures were determined. The DTA method was employed for the determination of the kinetic parameters of glass crystallization including the activation energy of crystal growth E_a.

A hot stage microscope (HSM), E. Leitz Wetzlar, supplied with a Cannon camera, was used for determining the sintering behavior of the glass powder samples [17–24]. The glass powder samples were pressed into cylinders. The specimens were placed on a platinum plate and then on an alumina support. The temperature was measured with a (Pt/Rh/Pt) thermocouple. The heating rate was 10 °C min^{-1}. The sample images were analyzed using computer software for image analyzing and the changes in the area at different heating temperatures were calculated.

The crystallization of bulk glass samples was performed by heating the samples in a Carbolite CWF 13/13 electric furnace with automatic regulation and a temperature accuracy of ± 1 °C, up to the crystallization temperatures determined by DTA, at a heating rate 10 °C min^{-1}, and maintained at these temperatures for different times. After the heat treatment, the samples were removed from the furnace and crushed.

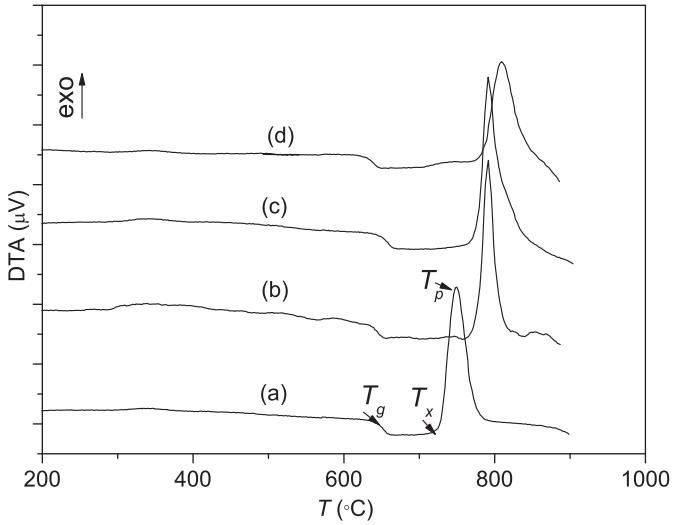

Fig. 1. DTA curves of the glass powder samples (a) GLa14.3, (b) GLa9.5, (c) GLa19.1, and (d) GLa5.7.

The XRD technique was used for identification of the crystalline phases in the powdered samples. The XRD patterns were obtained using a Philips PW-1710 automated diffractometer with a Cu tube operated at 40 kV and 30 mA. The instrument was equipped with a diffracted beam curved graphite monochromator and an Xe-filled proportional counter. The diffraction data were collected in the 2θ Bragg angles from 5 to 70°, counting for 1 s, except for the sample containing 14.3 mol% La_2O_3 (see Table 3).

A Jeol JSM-6610LV scanning electron microscope and a TOPCON transmission electron microscope (TEM) using the selected area electron diffraction (SAED) method were employed to observe the microstructure of the samples. Gold sputtered bulk samples were used for the SEM analyses. For the TEM observation, the powdered samples, obtained from heat treated bulk samples, were suspended in ethanol and mixed by ultrasound for 10 min and then applied to a copper grid coated with carbon.

3. Results and discussion

The compositions of the prepared glasses are given in Table 1. The samples were labeled depending on the amount of lanthanum oxide in the glass.

3.1. Differential thermal analyses

The DTA curves of the glasses are shown in Fig. 1. The small endothermic shoulders on the DTA curves represent the glass transition temperatures, T_g. The temperatures, T_x, crystallization onset, were determined by extrapolation. The exothermal temperature peaks T_p at the DTA curves correspond to the crystallization of glass. These characteristic temperatures are shown in Table 2.

It may be seen from Table 2 that the crystallization onset temperature, T_x, generally increased with increasing content of

lanthanum oxide. The sample GLa14.3, showing a lowest value of T_x, was the exception from this trend. An increasing trend of the T_g with increasing content of lanthanum oxide was also observed, with the same exception. The temperatures of glass crystallization, T_p, were approximately 800 °C, except for the T_p of GLa14.3, which was 749 °C. The parameter ΔT demonstrates the glass stability (GS). A larger temperature difference indicates a greater glass stability and smaller tendency toward crystallization. The smallest ΔT value was registered for the GLa14.3 glass, indicating its greatest trend toward crystallization.

3.2. Hot stage microscopy

In Fig. 2 are shown photomicrographs of the characteristic shape of the GLa14.3 taken during HSM experiments, which are representative for the other samples. The temperatures corresponding to typical viscosity points were determined from the photomicrographs. The temperature of the first shrinkage (T_{FS}) is temperature at which the sample shrinks to about 3–5% of its initial height, when the typical viscosity was $\log \eta = 9.1 \pm 0.1$, η is in dPa s. The temperature of maximum shrinkage (T_{MS}) is the temperature at which the sample shrinks to the maximum possible level, before softening, and a sample still has sharp edges, $\log \eta = 7.8 \pm 0.1$. T_D is the point at which the first signs of softening could be observed, the edges of the samples are rounded, $\log \eta = 6.3 \pm 0.1$. Moreover, T_S is the temperature at which the sample is spherical, $\log \eta = 5.4 \pm 0.1$, whereas the half-ball temperature (T_{HB}) is the temperature at which the section of the sample observed forms a semicircle, $\log \eta = 4.1 \pm 0.1$, and the flow temperature (T_F) is the temperature at which the maximum height of the drop of molten glass corresponds to a unit on the microscopic scale, $\log \eta = 3.4 \pm 0.1$ [17,18].

The characteristic temperature values for all glass samples obtained by HSM measurements are summarized in Table 2.

The temperature of the first shrinkage (T_{FS}) was 600 °C for the samples GLa5.7, GLa9.5 and GLa14.3, whereas for the sample GLa19.1, having the largest content of lanthanum oxide, it attained 680 °C. The temperatures of maximum sintering (T_{MS}) were in the range from 700 °C to 740 °C, increasing with increasing content of lanthanum oxide. The flow temperature (T_F) of glasses increased with increasing content of lanthanum oxide in the sample.

3.3. A combination of differential thermal analyses and hot stage microscopy

To analyze the sintering and crystallization behavior of glasses, the results of the HSM and DTA analyses, obtained in the same temperature range, are compared in Fig. 3. The sintering process of the glass powders is given as the change of the relative area A/A_0 of the samples as a function of temperature, where A_0 is the initial area and A is the area at temperature T. The shrinkage of the samples was determined by this ratio.

According to Fig. 3, the smallest shrinkage ($A/A_0 = 0.70$) was determined for the sample GLa19.1 with the highest content of lanthanum oxide. The maximum shrinkage ($A/A_0 = 0.54$) was observed for the sample GLa14.3. The physical processes that control the densification kinetics of porous glass bodies by reducing their surface energy are well studied. The glass particle surface energy is the driving force and the viscous flow is the kinetic path through which the surface area is reduced. However, during sintering, surface crystallization of glass particles as a concomitant process can occur and hence the sintering kinetics is retarded of even

Table 2
Characteristic temperatures obtained by DTA and HSM measurements at the 10 °C min^{-1} heating rate.

Temperatures (°C)	**Glass samples**			
	GLa5.7	**GLa9.5**	**GLa14.3**	**GLa19.1**
T_g	622	640	638	644
T_x	735	763	723	765
T_p	809	792	749	792
$\Delta T = (T_x - T_g)$	113	123	80	121
T_{FS}	600	600	600	680
T_{MS}	700	719	739	740
T_D	680	720	760	760
T_S (°C)	740	760	800	800
T_{HB}	840	900	1000	1050
T_F	890	950	1020	1060

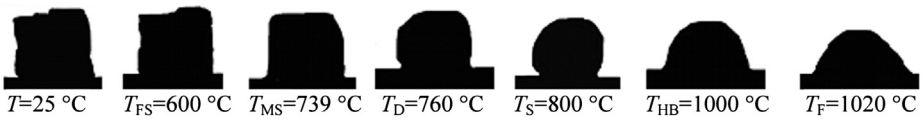

Fig. 2. Photomicrographs of the shape of GLa14.3 sample during the HSM measurements.

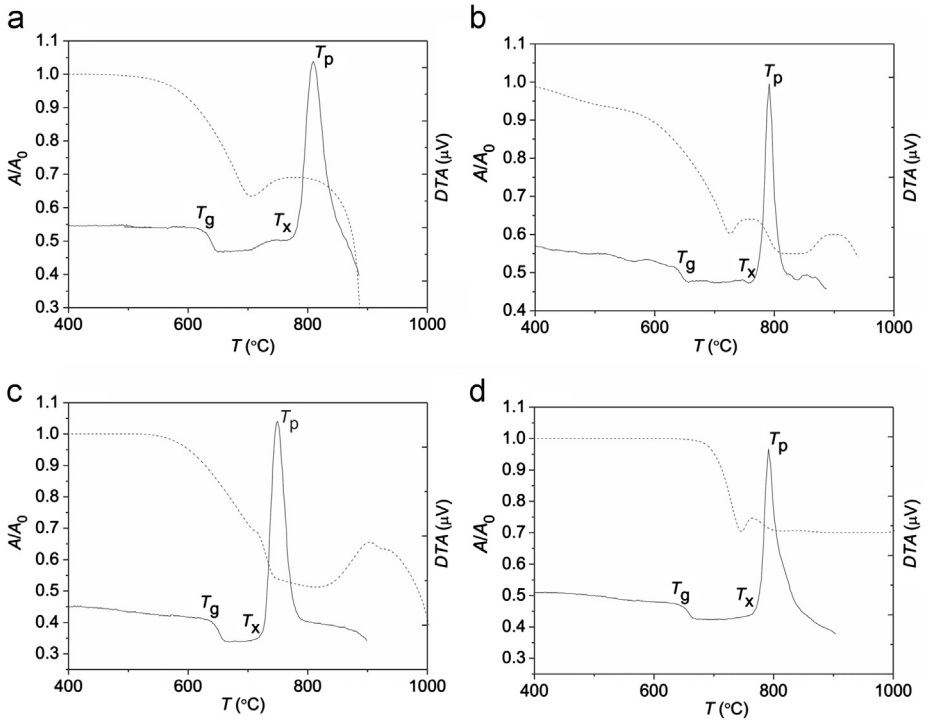

Fig. 3. HSM and DTA curves for glass powder samples (a) GLa5.7, (b) GLa9.5, (c) GLa14.3 and (d) GLa19.1.

inhibited [11,25,26]. As an indication that the sintering and crystallization processes proceed independently, the difference between T_x and T_{MS} can be considered. A bigger difference between these temperatures indicates that the glass powder will sinter before the crystallization process starts. In the case where the sintering process ends before crystallization starts, residual porosity of the glass body can be avoided and a dense glass-ceramics material can be obtained [27,28]. According to the DTA and HSM results (Table 2), for all the samples, except GLa14.3, T_x was greater than T_{MS}, which indicates independence of the sintering and crystallization processes. On the contrary, for the GLa14.3 sample, T_{MS} was higher than T_x and in such a case, the crystallization process starts before complete densification was reached Fig. 3c.

3.4. X-ray diffraction

To determine the phase composition of crystallized glass samples, XRD analysis was performed and the results are shown in Fig. 4.

The samples were heated at the crystallization temperatures determined by DTA. Thus, GLa5.7 was heated at 810 °C, GLa19.1 at 790 °C and GLa14.3 at 760 °C for 70 h. According to XRD patterns shown in Fig. 4, complex crystallization was observed in the samples GLa5.7 and GLa19.1. Two phases, $La_2SrB_{10}O_{19}$ [29] and SrB_6O_{10} (JCPDS 20-1190) [30] were identified in GLa5.7 after adequate heat treatment. The phases $La_2SrB_{10}O_{19}$ and $SrLaBO_4$ (JCPDS 34-1045) [31] were formed in GLa19.1. Only one phase, $La_2SrB_{10}O_{19}$, was formed in GLa14.3 indicating that polymorphic crystallization occurred in this sample.

The X-ray powder diffraction (XRD) method was used for the identification of the phase composition of the glass sample GLa14.3 and determination of the unit-cell parameters. The powder pattern was obtained using the experimental conditions described in Table 3. The unit-cell parameters were obtained using the LSUCRIPC (least square unit cell refinement) software [32].

The unit-cell parameters for $La_2SrB_{10}O_{19}$ were calculated using data for the same compound published by Cao et al. [29]. Moreover $La_2SrB_{10}O_{19}$ is isostructural with $La_2CaB_{10}O_{19}$ [33]. The observed and calculated XRD data for the synthesized compound that is the subject of this paper are given in Table 4, and the unit-cell parameters in comparison to the literature data are given in Table 5.

3.5. Scanning and transmission electron microscopy

Glasses with polymorphic crystallization are rare and for this reason a more detailed investigation including the mechanism and the kinetics of crystallization were undertaken on this sample. The SEM micrographs of the heat treated bulk GLa14.3 sample are shown in Fig. 5. From the SEM microphotographs (cross section), it can be observed that the surface crystallization mechanism was operative for this glass. The crystallized layer formed by the growth of $La_2SrB_{10}O_{19}$ crystals (XRD, Fig. 4b) from the sample surface is clearly visible. A plate-like morphology of these crystals was observed, Fig. 5.

The polymorphic crystallization of GLa14.3 glass was also confirmed by TEM/SAED analysis. By TEM analysis, crystallites distributed in the glass matrix were identified in the sample heat-treated for 30, 60 and 90 min, (Fig. 6a,b and c). Based on the SAED diffraction pattern, the determined unit cell parameters a, b and β were in good agreement with those reported for the $La_2SrB_{10}O_{19}$ phase, *i.e.*, 11.16 Å assigned to the a, 6.58 Å assigned to the b and 91.44° assigned to the β [34].

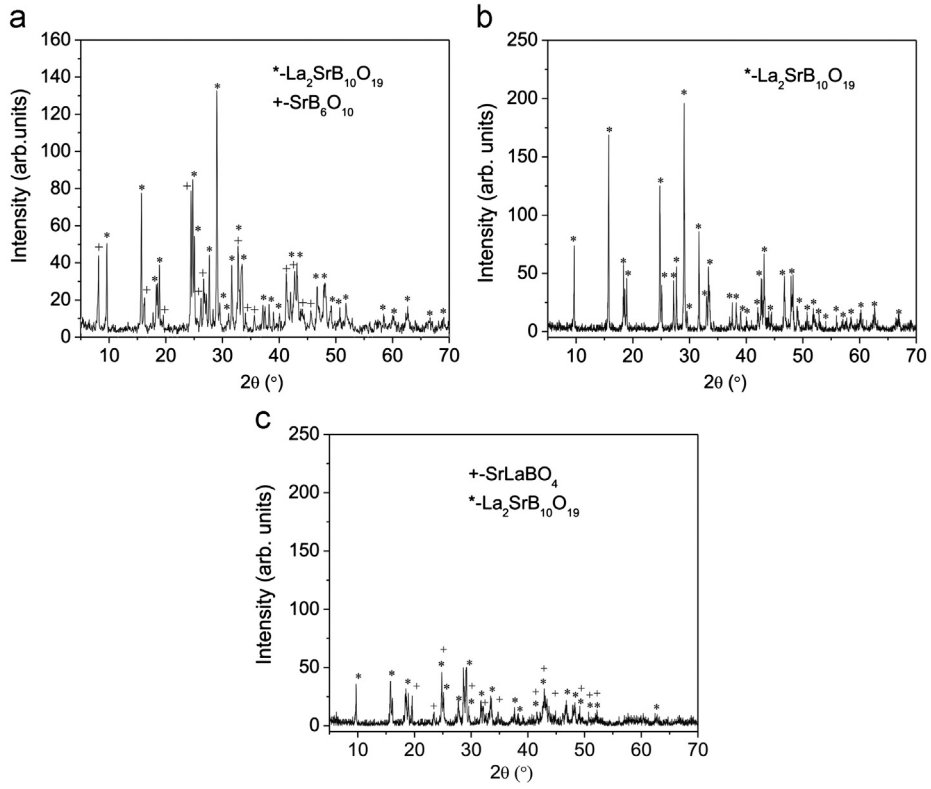

Fig. 4. XRD patterns of the heat-treated glass samples (a) GLa5.7, (b) GLa14.3, and (c) GLa19.1.

Table 3
X-ray powder diffraction data for $La_2SrB_{10}O_{19}$.

Sample characterization			
Name (chemical, mineral)	Dilanthanum strontium decaborate		
Empirical formula	$La_2SrB_{10}O_{19}$		
Source/preparation	Synthetic		
Technique			
Radiation type, source	X-rays, Cu λ value used 1.54060 Å Kα_1/1.54439 Kα_2		
Monochromator	Diffracted beam	Graphite monochromator	
Detector (film, scint. *etc*.)	Proportional		
Instrument description (type, slits)	Vertical diffractometer Divergence slit 1° Receiving slit 0.1 mm Soller slit 1°		
Instrumental profile breadth	0.10° 2θ	temp. (°C)	25 ± 1
Specimen form/particle size	Edge loaded powder/ < 10 μm particle size		
Range of 2θ	From 5 to 75° 2θ		
Specimen motion	None		
Unit-cell data			
Unit-cell parameters	a=11.065(3), b=6.564(2), c=9.225(3) Å, β=91.09(2) °, V=669.9(2) Å^3, Z=2, D_x=3.855 g cm^{-3}		
Formula wt.	777.52 g mol^{-1}		
Crystal system	Monoclinic		
Space group	$C2$ (5)		
	Least square unit-cell refinement method		

The GLa14.3 glass-ceramic obtained by sintering the glass powder (particle size < 0.1 mm) was also analyzed using SEM. The SEM micrographs of free and fractured sample surface are shown in Fig. 7. From the presented micrographs, it is obvious that a non-homogenous and porous glass-ceramic body was obtained. In Fig. 7a, the interconnected glass particles and pores (black spots) are visible in Fig. 7a. Under high magnification, Fig. 7b, crystallites on particle surface are visible. The fractured

Table 4
Comparison of the calculated and observed XRD data for $La_2SrB_{10}O_{19}$.

I_{rel} (%)	$h\ k\ l$	d_{calc} (Å)	d_{obs} (Å)	I_{rel} (%)	$h\ k\ l$	d_{calc} (Å)	d_{obs} (Å)
23	0 0 1	9.222	9.199	11	−4 2 2	1.933	1.931
56	1 1 0	5.645	5.640	35	5 1 2	1.895	1.896
24	−1 1 1	4.835	4.830	20	0 2 4	1.887	1.887
15	−2 0 1	4.781	4.773	24	3 3 0	1.882	1.884
30	2 0 1	4.703	4.686	13	3 1 4	1.859	1.857
70	−1 1 2	3.588	3.586	11	6 0 0	1.843	1.845
30	1 1 2	3.554	3.551	10	3 3 1	1.840	1.842
25	0 2 0	3.282	3.278	10	−4 0 4	1.787	1.788
30	3 1 0	3.214	3.216	17	−2 0 5	1.760	1.762
100	0 0 3	3.074	3.069	12	4 0 4	1.754	1.757
15	3 1 1	3.019	3.016	8	−4 2 3	1.754	1.751
40	2 2 0	2.822	2.820	7	4 2 3	1.730	1.730
20	−2 2 1	2.706	2.707	5	0 4 0	1.641	1.641
32	2 2 1	2.692	2.689	7	−3 3 3	1.612	1.614
30	−4 0 1	2.662	2.665	6	6 2 0	1.607	1.609
28	3 1 2	2.616	2.620	4	3 3 3	1.598	1.598
8	−2 2 2	2.418	2.421	5	6 2 1	1.579	1.578
15	2 2 2	2.397	2.395	8	−1 3 4	1.574	1.575
15	−4 0 2	2.391	2.392	4	−4 2 4	1.570	1.569
16	4 0 2	2.351	2.349	4	−2 2 5	1.551	1.550
14	0 0 4	2.306	2.305	5	5 3 1	1.530	1.533
8	0 2 3	2.244	2.247	4	4 0 5	1.521	1.522
10	−3 1 3	2.240	2.244	3	−7 1 1	1.519	1.520
3	3 1 3	2.203	2.199	4	−2 4 2	1.492	1.493
12	−1 3 0	2.147	2.146	8	2 4 2	1.487	1.485
13	1 1 4	2.127	2.124	12	1 1 6	1.479	1.481
25	2 0 4	2.114	2.116	7	−5 3 2	1.480	1.479
30	4 2 0	2.114	2.111	4	3 3 4	1.451	1.451
35	5 1 0	2.096	2.097	3	6 2 3	1.415	1.415
8	−4 2 1	2.067	2.069	6	−2 4 3	1.404	1.406
12	4 2 1	2.054	2.056	8	−4 2 5	1.400	1.400
7	−5 1 1	2.051	2.051	5	−5 1 5	1.397	1.397
7	5 1 1	2.036	2.037	5	0 4 4	1.337	1.336
36	1 3 2	1.943	1.941	7	6 2 4	1.308	1.309

Table 5
The determined unit-cell parameters in comparison to literature data.

Compound	a (Å)	b (Å)	c (Å)	β (°)	V (Å^3)	Literature
$La_2SrB_{10}O_{19}$	11.065(3)	6.564(2)	9.225(3)	91.09(2)	669.9(2)	This study
$La_2SrB_{10}O_{19}$	11.054(1)	6.556(9)	9.235(6)	90.91	–	[26]
$La_2CaB_{10}O_{19}$	11.043(3)	6.563(2)	9.129(2)	91.47	661.4(3)	[27]

surface revealed a porous structure containing large voids (black spots). As in the case of bulk glass sample (Fig. 5), a plate-like crystal morphology was observed for the surface crystallized glass particles, Fig. 7a,b. These crystals were previously determined as $La_2SrB_{10}O_{19}$ (XRD, Fig. 4b) and in such a way, the polymorphic crystallization of the GLa14.3 glass was confirmed.

3.6. Kinetic parameters of crystallization

Further investigation of the crystallization of GLa14.3 was focused on determining kinetic parameters of crystallization. Kinetic parameters were determined by DTA based on the crystallization peaks, Fig. 8.

The temperatures of the crystallization peaks in dependence on the heating rate are given in Table 6.

The temperature of the crystallization peak, T_p, increased with increasing heating rate. Calculation of kinetic parameters was based on the modified form of the Kissinger equation proposed by Matusita and Sakka [35]

$$\ln\left(\frac{\beta^n}{{T_p}^2}\right) = -\frac{mE}{RT_p} + k \quad (1)$$

where R is the gas constant, β is the heating rate, T_p is the temperature of the crystallization peak and k is a constant. The constant n is known as the Avrami parameter and m represents the dimensionality of crystal growth. The values of

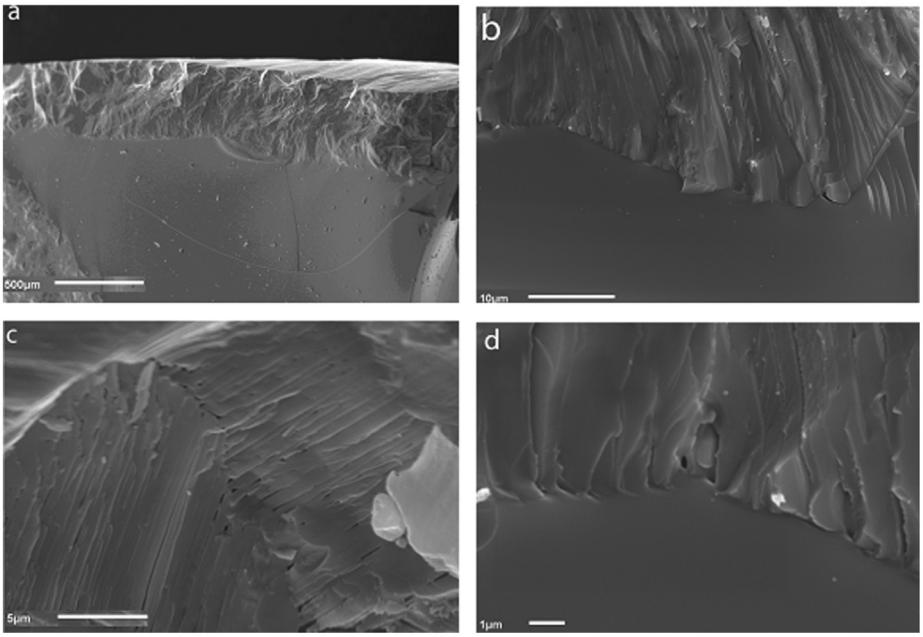

Fig. 5. SEM microphotographs of the GLa14.3 glass heat treated at $T=760$ °C for $t=90$ min (a) surface crystallized layers, (b) glass/crystal interface and (c) and (d) plate-like crystal morphology.

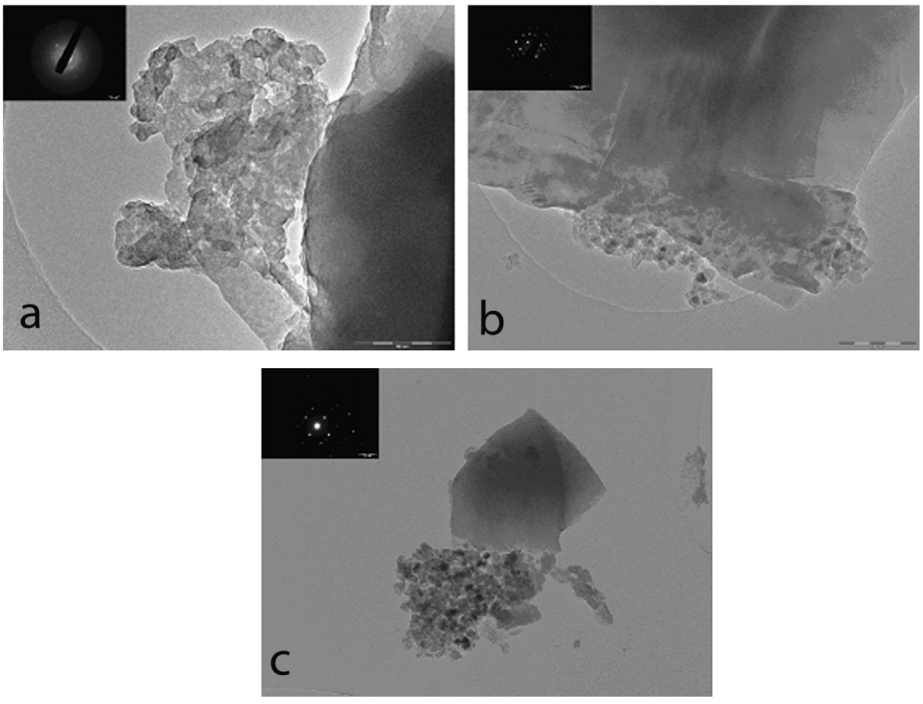

Fig. 6. TEM/SAED images of the GLa14.3 glass heat-treated at $T=760$ °C for t (a) 30 min, (b) 60 min and (c) 90 min.

parameters n and m depend on the crystallization mechanism. The E values were obtained from plots of $\ln(\beta^n/T_p^2)$ vs. $1/T_p$, using appropriate values of n and m. If the experiments were performed in such a way that the glass samples were saturated with nuclei prior to crystal growth, then parameter E can be interpreted as the activation energy of crystal growth [36,37]. XRD analysis showed that this glass crystallized polymorphic. In this case, the chemical composition of the melt and the crystal are the same and the crystal growth rate is controlled by interface reactions. SEM results showed that this glass crystallized by the surface mechanism. Therefore, to satisfy the condition of a constant number of nuclei during crystal growth, the glass powder with the smallest particle size of < 0.048 mm was chosen for this experiment. In the range of the smallest granulation, the number of surface with respect to internal nuclei is dominant in the total number of nuclei present. In

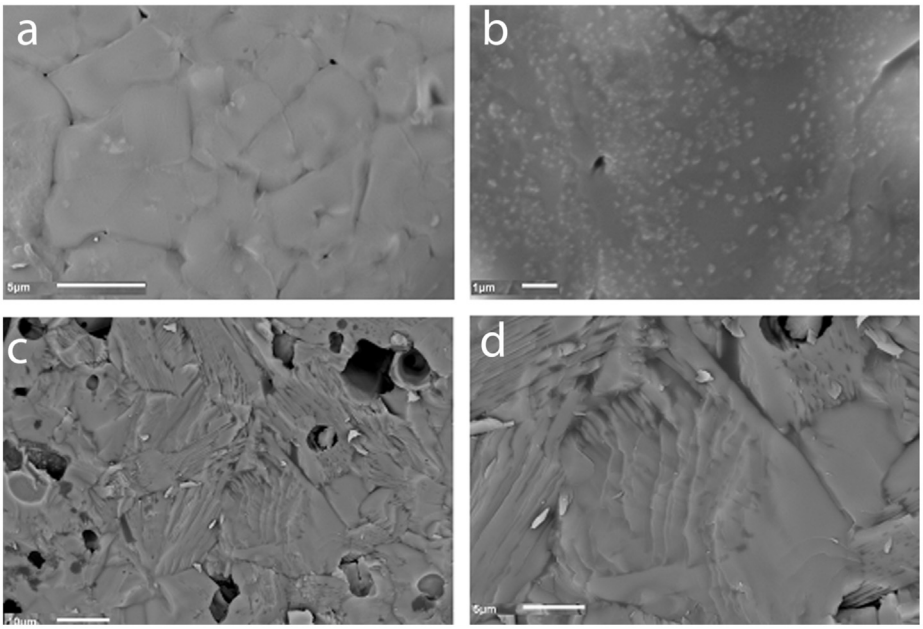

Fig. 7. SEM micrograph of the GLa14.3 obtained by sintering the glass powder at $T=760$ °C for $t=90$ min. Free surface (a) and (b) and fractured surface (c) and (d).

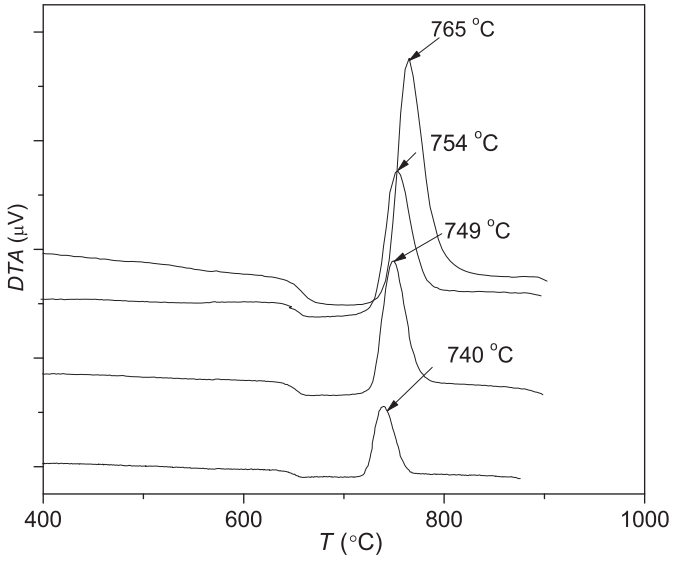

Fig. 8. DTA curves of powder samples grain size <0.048 mm, recorded for the GLa14.3 at different heating rates.

Table 6
Temperature of crystallization peaks, T_p for the glass powder sample GLa14.3 heated at different heating rates, β.

β (°C min^{-1})	5	10	12	20
T_p (°C)	740	749	754	765

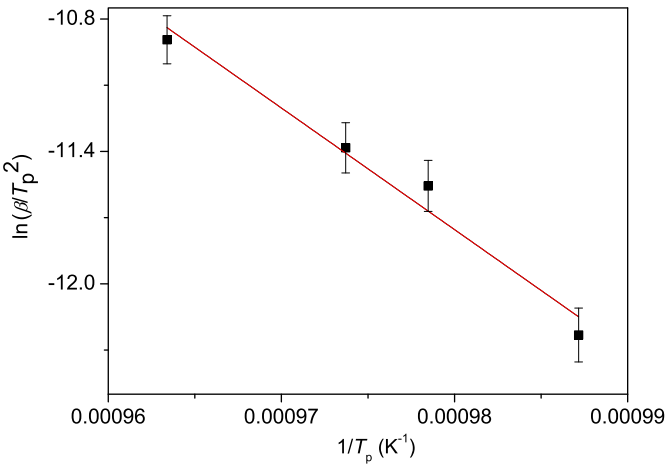

Fig. 9. The Kissinger plot $\ln(\beta/T_p^2)$ vs. $1/T_p$.

such a case, the crystal growth in DTA experiments occurred on a constant number nuclei, $n=m=1$ and Eq. (1) becomes the same as the well-known Kissinger equation [38]. The Kissinger plot, $\ln(\beta/T_p^2)$ vs. $1/T_p$ is shown in Fig. 9. An activation energy E of crystal growth was calculated from the slope of the line, $E_a=458\pm63$ kJ mol^{-1}.

The Ozawa method can also be applied in this case for the calculation of the activation energy [39]

$$\ln(\beta) = -(E_{oz}/RT_p) + \text{const} \quad (2)$$

The value of the activation energy calculated by application of the Ozawa method was $E_{oz}=475\pm63$ kJ mol^{-1}, which is in good agreement with that obtained by the Kissinger method.

4. Conclusions

The crystallization and sinterability of glass in the ternary system La_2O_3–SrO–B_2O_3 for glass powder and bulk glass samples were studied. The glass powder samples were studied by DTA and HSM. The lowest glass stability was shown by

the GLa14.3 glass sample. For this glass, $T_{MS} > T_x$, meaning that the sintering and crystallization processes were not independent.

XRD analysis of the crystallized glass samples identified $La_2SrB_{10}O_{19}$ and SrB_6O_{10} in GLa5.7, and $La_2SrB_{10}O_{19}$ and $SrLaBO_4$ in GLa19.1. XRD and TEM/SAED analyses confirmed the polymorphic crystallization with precipitation of $La_2SrB_{10}O_{19}$ in the GLa14.3 glass sample. Surface crystallization was evidenced from the SEM images of this glass. A non-homogenous and porous glass-ceramics body were obtained by powder sintering of the GLa14.3 glass at $T=760\ ^{\circ}C$ for $t=90$ min. An activation energy of crystal growth $E_a=458\pm63$ kJ mol^{-1} was calculated using the Kissinger method, which was in good agreement with the activation energy, $E_{oz}=475\pm63$ kJ mol^{-1} obtained by application of the Ozawa relation.

Acknowledgment

The authors are grateful to the Ministry of Education, Science and Technological Development of the Republic of Serbia for financial support (Projects 172004 and 34001).

References

[1] W. Holand, G. Beall, Glass-Ceramic Technology, second ed., The American Ceramic Society, Ohio, 2012.
[2] S. Banijamali, H.R. Rezaei, B. Eftekhari Yekta, V.K. Marghussian, Crystallization and properties of glass-ceramic tiles belonging to CaF_2–CaO–MgO–Al_2O_3–SiO_2 system, Ceramics Interational 33 (2007) 1557–1561.
[3] R. Rajaramakrishna, S. Karuthedath, R.V. Anavekar, Nonlinear optical studies of lead lanthanum borate glass doped with Au nanoparticles, Journal of Non-Crystalline Solids 358 (2012) 1667–1672.
[4] I. Dyamant, E. Korin, J. Hormadaly, Thermal and some physical properties of glasses in the La_2O_3–CaO–B_2O_3 ternary system, Journal of Non-Crystalline Solids 354 (2008) 3135–3141.
[5] I. Dyamant, E. Korin, J. Hormadaly, Non-isothermal crystallization kinetics of $La_2CaB_{10}O_{19}$ from glass, Journal of Non-Crystalline Solids 357 (2011) 1690–1695.
[6] I. Dyamant, E. Korin, J. Hormadaly, Characteristic of $La_2CaB_{10}O_{19}$ from glass, Journal of Non-Crystalline Solids 356 (2010) 1784–1790.
[7] G. Kaur, O.P. Pandey, K. Singh, Effect of modifiers field strength on optical, structural and mechanical properties of lanthanum borosilicate glasses, Journal of Non-Crystalline Solids 358 (2012) 2589–2596.
[8] M. Romero, M. Kovacova, J.M. Rincón, Effect of particle size on kinetic crystallization of an iron-rich glass, Journal of Materials Science 43 (2008) 4135–4142.
[9] M. Aloisi, A. Karamanov, G. Taglieri, F. Ferrante, M. Pelino, Sintered glass ceramic composites from vitrified municipal solid waste bottom ashes, Journal of Hazardous Materials 137 (2006) 138–143.
[10] M. Romero, R.D. Rawlings, J.M. Rinc, Crystal nucleation and growth in glasses from inorganic wastes from urban incineration, Journal of Non-Crystalline Solids 271 (2000) 106–118.
[11] A.R. Boccaccini, W. Stumpfe, D.M.R. Taplin, C.B. Ponton, Densification and crystallization of glass powder compacts during constant heating rate sintering, Materials Science and Engineering: A 219 (1996) 26–31.
[12] C. Siligardi, J.P. Wu, A.R. Boccaccini, Sintering and crystallization of vanadium doped CaO–ZrO_2–B_2O_3, Materials Letters 60 (2006) 1607–1612.
[13] H.R. Fernandes, D.U. Tulyaganov, M.J. Pascual, V.V. Kharton, A. A. Yaremchenko, J.M.F. Ferreira, The role of K_2O on sintering and crystallization of glass powder compacts in the Li_2O–K_2O–Al_2O_3–SiO_2 system, Journal of the European Ceramic Society 32 (2012) 2283–2292.
[14] C.L. Chen, W.C.J. Wei, A. Roosen, Wetting, densification and phase transformation of La_2O_3/Al_2O_3/B_2O_3-based glass-ceramic, Journal of the European Ceramic Society 26 (2006) 59–65.
[15] R.C.C. Monteiro, A.A.S. Lopes, M.M.A. Lima, J.P. Veiga, R.J.C. Silva, C.J. Dias, E.J.R. Davim, M.H.V. Fernandes, Sintering, crystallization, and dielectric behavior of barium zinc borosilicate glasses–effect of barium oxide substitution for zinc oxide, Journal of the American Ceramic Society 95 (2012) 3144–3150.
[16] Y.H. Jo, S.H.N. Doo, J.S. Lee, B.C. Mohanty, Y.S. Cho, Effect of Zn and Ca modifications on crystallization and microwave dielectric properties of lanthanum borates, Journal of Alloys and Compounds 509 (2011) 849–853.
[17] C. Lara, M.J. Pascual, M.O. Prado, A. Duran, Sintering of glasses in the system RO–Al_2O_3–BaO–SiO_2 (R = Ca, Mg, Zn) studied by hot stage microscopy, Solid State Ionics 170 (2004) 201–208.
[18] M.J. Pascual, A. Duran, M.O. Prado, A New, Method for determining fixed viscosity points of glasses, Physics and Chemistry of Glasses 46 (2005) 512–520.
[19] C. Lara, M.J. Pascual, A. Duran, Glass-forming ability, sinterability and thermal properties in the system RO–BaO–SiO_2 (R = Mg, Zn), Journal of Non-Crystalline Solids 348 (2004) 149–155.
[20] A.R. Boccaccini, B. Hamann, Review in situ high-temperature optical microscopy, Journal of Materials Science 34 (1999) 5419–5436.
[21] M. Paganelli, D. Sighinolfi, Understanding the behavior of glazes with the automatic heating microscope, Ceramic Forum International/Ber. DKG 85 (2008) E63–E67.
[22] H. Nonnet, H. Khedim, F.O. Mear, Development and characterization of glass ceramic sealants for solid oxide electrolyser cells, Ionics 18 (2012) 441–447.
[23] S.T. Reis, M.J. Pascual, R.K. Brow, C.S. Ray, T. Zhang, Crystallization and processing of SOFC sealing glasses, Journal of Non-Crystalline Solids 356 (2010) 3009–3012.
[24] P.K. Ojaha, T.K. Chongdar, N.M. Gokhale, A.R. Kulkarni, Investigation of crystallization of La_2O_3–SrO–B_2O_3–SiO_2 glass and its suitability for SOFC, International Journal of Hydrogen Energy 36 (2011) 14996–15001.
[25] M.O. Prado, M.L.F. Nascimento, E.D. Zanotto, On the sinterability of crystallizing glass powders, Journal of Non-Crystalline Solids 354 (2008) 4589–4597.
[26] M.O. Prado, E.D. Zanotto, Glass sintering with concurrent crystallization, Comptes Rendus Chimie 5 (2002) 773–786.
[27] C. Siligardi, M.C. D'Arrigo, C. Leonelli, Sintering behavior of glass-ceramic frits, American Ceramic Society Bulletin 79 (2000) 88–92.
[28] E.D. Zanotto, V.M. Fokin, Recent studies of internal and surface nucleation insilicate glasses, Philosophical Transactions of the Royal Society of London, Series A 361 (2003) 591–613.
[29] J. Cao, J. Wang, P. Fu, F. Guo, Z. Yang, Y. Wu, Synthesis and characterization of a novel non-linear optical material $La_2SrB_{10}O_{19}$, Progress in Crystal Growth and Characterization of Materials 40 (2000) 97–101.
[30] Joint Committee on Powder Diffraction Standards (JCPDS), Powder Diffraction Data, Card no. 20-1190, Swarthmore, PA.
[31] Joint Committee on Powder Diffraction Standards (JCPDS), Powder Diffraction Data, Card no. 34-1045, Swarthmore, PA.
[32] R.G. Garvey, LSUCRIPC least square unit-cell refinement with indexing a personal computer, Powder Diffraction 1 (1986) 114.
[33] Y. Wu, J. Liu, P. Fu, J. Wang, H. Zhou, G. Wang, C. Chen, A new lanthanum and calcium borate $La_2CaB_{10}O_{19}$, Chemistry of Materials 13 (2001) 753–755.
[34] D.B. Williams, C.B. Carter, Transmission Electron Microscopy a Text Book For Materials Science, Springer, New York, USA, 2009.
[35] K. Matusita, S. Sakka, Kinetic study on crystallization of glass by differential thermal analysis—criterion on application of Kissinger plot, Journal of Non-Crystalline Solids 38–39 (1980) 741–746.
[36] M.C. Weinberg, On the analysis of non-isothermal thermoanalytic crystallization experiments, Journal of Non-Crystalline Solids 127 (1991) 151–158.
[37] K.F. Kelton, Analysis of crystallization kinetics, Materials Science and Engineering A 226–228 (1997) 142–150.
[38] H.E. Kissinger, Reaction kinetics in differential thermal analysis, Analytical Chemistry 29 (1959) 1702–1706.
[39] T. Ozawa, A modified method for kinetic analysis of thermoanalytical data, Journal of Thermal Analysis 9 (1976) 369–373.